DTX3L and USP28 fine-tune DNA double strand repair through mutual regulation of their protein levels

Yashwanth Ashok[#,1], Daniela Mennerich[#, 1], Carlos Vela-Rodríguez [1], Heli I. Alanen [1], Melanie Rall-Scharpf [2], Lisa Wiesmüller[2], Renata Prunskaite-Hyyryläinen[1], Lari Lehtiö[*,1] & Thomas Kietzmann[*,1]

[1]Faculty of Biochemistry and Molecular Medicine and Biocenter Oulu, University of Oulu, Oulu, Finland

[2]Department of Obstetrics and Gynecology, Ulm University, Ulm, Germany

# Both the authors contributed equally.

* Corresponding authors: lari.lehtio@oulu.fi, thomas.kietzmann@oulu.fi

Abstract

The DNA damage response involves a complex protein network with members mediating different post-translational modifications such as ubiquitination and deubiquitination. Thereby the E3 ubiquitin ligase DTX3L as well as the deubiquitinase USP28 are recruited especially to DNA double strand breaks (DSBs) suggesting mutual functional interactions. Here we present evidence for the existence of such crosstalk. Mechanistically we show that DTX3L interacts with USP28 and ubiquitinates it, which leads to its proteasomal degradation. Vice versa, USP28 can remove those polyubiquitin chains from itself as well as from autoubiquitinated DTX3L. Consequently, these mutual regulatory interactions between DTX3L and USP28 affected DSB repair activities. Analysis of distinct DSB repair pathways reveals synthetic dysfunction of canonical non-homologues end joining (NHEJ) and homologous recombination (HR), upon USP28 and DTX3L double knockdown, suggesting cooperation between these proteins. Conversely, error-prone microhomology-mediated end joining (MMEJ) requires USP28 to counterbalance the antagonistic DTX3L effect. Together, the present data indicate that DTX3L and USP28 are under mutual control to fine-tune the capacity and quality of the cellular responses to stresses such as DNA damage.

Running title: DTX3L and USP28 fine-tune DNA repair

Keywords: Ubiquitination, DTX3L, USP28, hypoxia, c-MYC

Introduction

Ubiquitination is a posttranslational protein modification that involves the covalent attachment of ubiquitin molecules to target proteins, leading either to their degradation by the proteasome or the regulation of a vast array of cellular processes.

Three different types of ubiquitinations are known: (a) monoubiquitination, (b) multi-monoubiquitination (c) polyubiquitination. While monoubiquitination mainly affects protein localization, polyubiquitination is best known for its regulation of protein abundance by promoting proteasomal degradation of polyubiquitinated proteins. However, it has recently emerged that polyubiquitination can have non-proteolytic functions by taking part in transcription regulation, inflammation, endocytosis, mitophagy, cell division and DNA repair (1). While the sequential action of three enzymes (E1, E2, and E3) is required for successful attachment of ubiquitin to a substrate, the substrate specificity is lastly determined by the E3 ubiquitin ligase (1).

Apart from the actual ubiquitination, there are other ubiquitin-like modifiers (UBLs) such as NEDD8, SUMO, and ISG15 that can also be conjugated to ubiquitin and target proteins to modulate their activity and localization. The latter may lead to formation of hybrid chains consisting, for example, of both ubiquitin and NEDD8 molecules. Overall, the presence of multiple types of UBLs and the formation of hybrid chains adds complexity to the regulation of protein degradation and cellular signaling (2).

Recently, one member of the DTX family of E3 ubiquitin ligases (3), DTX3L, has emerged to be involved in several diseases such as inflammation and cancer that are linked to differentiation, apoptosis, and DNA repair. However, the knowledge of DTX substrates and their molecular mechanisms is limited. DTX3L was originally identified as a binding partner of PARP9 (BAL1/ARTD9) and linked to DNA repair due to its ability to monoubiquitinate histone 4 and to promote recruitment of the tumor suppressor (TP53BP1) to DNA damage sites (4). In addition to DTX3L, there are other human E3 ligases (DTX1, DTX2, DTX3, and DTX4) which share a common C-terminal DTC domain that can catalyze ADP-ribosylation of ubiquitin independent of PARP9 (5). Moreover, DTX3L was found to be able to undergo autoubiquitination and to carry out poly-ubiquitination with different ubiquitin linkages (6, 7). However, the functional relevance especially with DNA repair remains to be determined (8).

Deubiquitinases (DUBs) reverse the ubiquitination process. In humans, there are about 100 enzymes that catalyze ubiquitin removal from substrates. DUBs are grouped into seven main classes based on their sequence relationship and structural fold. The first class is Ubiquitin-Specific Proteases (USPs), which is the largest class and cleaves ubiquitin from proteins using a conserved USP domain. The second class is Ubiquitin C-Terminal Hydrolases (UCHs), which remove ubiquitin from the C-terminus of proteins and consists of four members. Ovarian Tumor Domain Proteases (OTUs) form the third class, encompassing approximately 15 members that possess an OTU domain. The fourth class is Josephins, including ataxin-3 and ataxin-3-like protein, which are associated with neurodegenerative diseases. Machado-Joseph Domain Proteins (MJDs), the fifth class, also comprises ataxin-3 and ataxin-3-like protein, and is involved in neurodegeneration. JAB1/MPN/MOV34 Metalloenzymes (JAMMs), the sixth

class, are metalloprotease DUBs utilizing zinc ions coordinated by JAMM motifs. The seventh class, Monocyte Chemotactic Protein-Induced Proteins (MCPIPs), consists of MCPIP1 and MCPIP2, and they play roles in immune and inflammatory responses. These distinct classes of DUBs highlight the diversity and complexity of the deubiquitination process in cellular regulation (9, 10).

Although some general understanding about the function of DUBs exists, not much is known about the specific roles of many family members. From those, ubiquitin-specific protease 28 (USP28) encoded at chromosome 11q23 has recently gained interest as it was implicated to modulate several cellular processes such as DNA damage response, cell-cycle, and tumorigenesis. So far, two USP28 isoforms could be identified; the ubiquitously expressed canonical isoform and the 62 amino acids longer tissue-specific isoform that is found in muscles, heart and brain (11).

Like with DTX3L, the biological role of USP28 is connected to the DNA damage response, which is illustrated by the fact that USP28 is recruited to DNA damage sites (12, 13). USP28´s activity in response to DNA damage is tightly regulated by the ATM kinase that phosphorylates serine 67 and 714 leading to an increase in its catalytic activity (13). By contrast, cleavage of USP28 by caspase-8 causes loss of its catalytic activity and progression of the cell-cycle beyond the p53-dependent G2/M DNA damage checkpoint (14). Similarly, sumoylation of lysine 99 in the N-terminus of USP28 was shown to reduce USP28 activity, whereas the SUMO protease SENP1 could reverse this effect under hypoxic conditions (15). In addition, USP28 was shown to interact with TP53BP1 and to rescue it from degradation along with other proteins involved in the DNA damage response such as p53, claspin, and CHK2 (13, 16, 17). Within this scenario, the specific recruitment of the USP28 interactor TP53BP1 to DNA damage sites, specifically to DNA double strand breaks (DSBs) is promoted by a heterodimeric complex consisting of the ADP-ribosyltransferase PARP9 and the E3 ubiquitin ligase DTX3L (7). Considering this, we hypothesized that USP28 could oppose the action of DTX3L; Vice versa DTX3L could potentially ubiquitinate and affect USP28 function or levels. Consequently, this interplay could impact DNA DSB repair.

Here we uncover that USP28 is indeed able to deubiquitinate DTX3L. At the same time, we show that DTX3L ubiquitinates USP28 and promotes its proteasomal degradation. We also show that regulation of USP28 by DTX3L has functional consequences on known USP28 substrates such as TP53, c-MYC and HIF-1α as well as on DSB repair pathway usage. Together, these data indicate that the interplay between USP28 and DTX3L is critical for the DNA damage response and its perturbation during tumorigenesis.

Results

DTX3L and USP28 show physical interaction

To expand our understanding of the relationship between DTX3L and USP28, we first performed immunofluorescence microscopy experiments to test whether the two proteins colocalize. The analyses show that both proteins localize to the nucleus and as indicated by a

focal pattern particularly to certain sub-compartments **(Fig. 1A)**. These data are in line with gene ontology based functional enrichment analyses of the two proteins and their potential interactor TP53BP1 also suggesting an involvement in DNA repair (7, 13).

To further test the hypothesis that these proteins are components of the same complexes, we next performed immunoprecipitation experiments. To this end, we used HEK293 cells or SK-MES1 lung cancer cells fostering protein interactions by crosslinking and inhibiting proteasomal degradation by MG132 treatment. Protein extracts from those cells were used to perform co-immunoprecipitation assays with control IgG or antibodies against TP53BP1 and USP28. Indeed, we could detect both DTX3L and USP28 in the respective TP53BP1 immunoprecipitates **(Fig. S1**). We also performed immunoprecipitations without prior crosslinking by using HEK293 cells that were transfected with vectors allowing expression of HA-tagged DTX3L and FLAG-tagged USP28. After DTX3L was immunoprecipitated with HA-tag antibodies the subsequent western blot analyzes with FLAG-tag antibodies revealed presence of USP28 in the precipitates **(Fig. 1B**). To further substantiate these results at the endogenous level, we next used control IgG and an USP28 antibody for the immunoprecipitations and analysed the precipitates by western blotting with an antibody against DTX3L or USP28. The assay revealed a weak positive DTX3L band in the precipitates from the USP28 antibody but not in the IgG controls **(Fig. 1C**) again indicating a interaction between USP28 and DTX3L.

To further verify the USP28-DTX3L interaction and to determine their binding affinity in solution, we next expressed both proteins recombinantly and performed interaction measurements with microscale thermophoresis (MST). Therein, we titrated fluorescently labelled DTX3L with USP28 to determine their dissociation constant (K_d). CD spectra for USP28 were recorded to assess the degree of folding of the recombinantly produced proteins (Fig. S2). Although the curves did not reach complete saturation due to the high protein concentration required, the data show that the K_d value was in the µM range (4.9 ± 3.3 µM) (**Fig. 1C and Fig. S3**). Together, the data support the view that USP28 and DTX3L can interact in a direct manner.

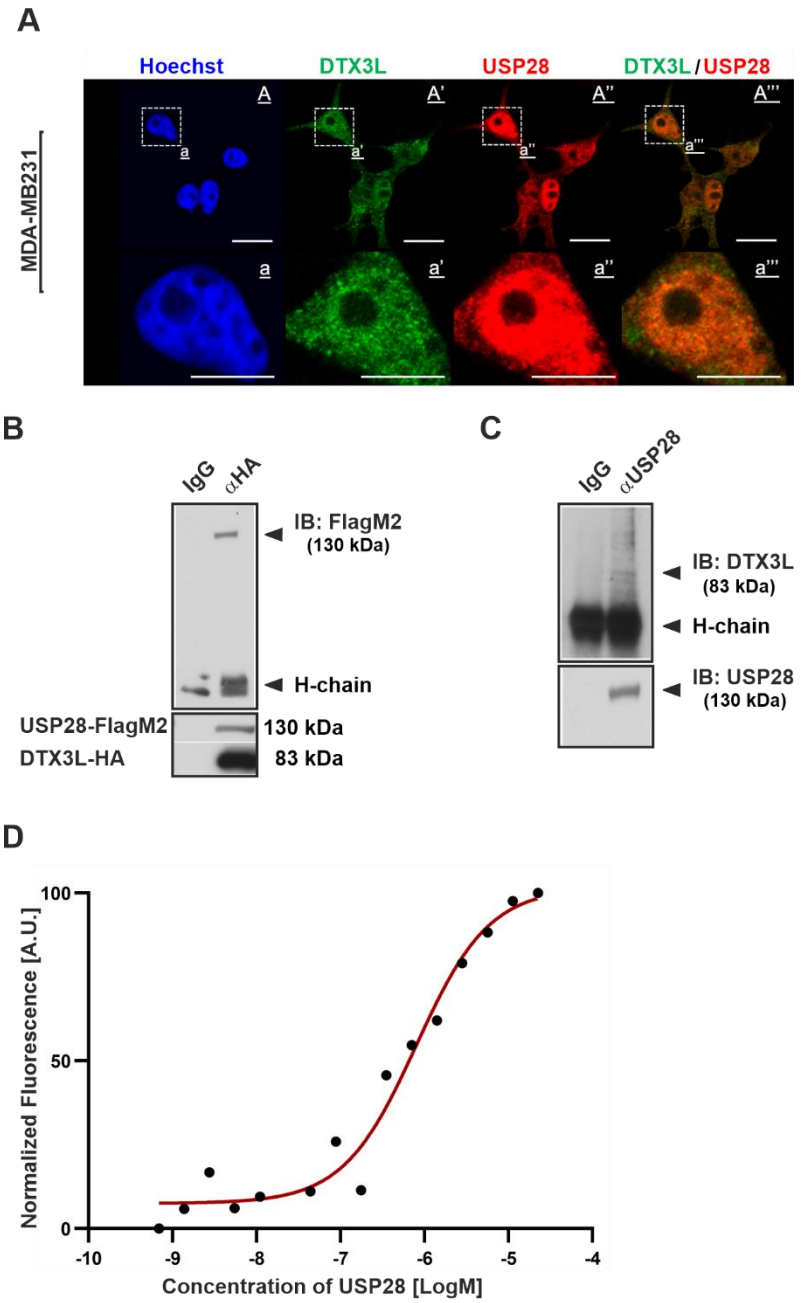

Figure 1. DTX3L and USP28 co-localize and interact with each other. A) Immunostaining with DTX3L (green) and USP28 (red) antibodies in MDA-MB231 cells shows that both proteins are co-expressed in the same cellular compartments. DAPI stained nuclei are shown in blue. Scale bars: A-A'' 20 µm and a-a''' 10 µm B) HEK293 cells were transfected with expression vectors encoding HA-tagged DTX3L and FLAG-tagged USP28. DTX3L was immunoprecipitated with HA-tag antibodies and precipitates were analyzed by western blotting using FLAG-tag antibodies. C) Cells were immunoprecipitated with control IgG or an USP28 antibody and precipitates were analyzed with an DTX3L antibody. Arrows point to specific bands. D) Representative MST binding curve for DTX3L and USP28 interaction.

USP28 can remove poly-ubiquitin (poly-Ub) chains catalyzed by DTX3L

Having shown that DTX3L and USP28 may reside even in the same complex and knowing that DTX3L undergoes auto-ubiquitination from our earlier report (6) we sought to investigate whether USP28 could catalyze removal of poly-Ub chains from DTX3L. To test this idea, we used full-length DTX3L as a substrate in an *in vitro* ubiquitination assay. In agreement with our previous report, the assay revealed that DTX3L was able to undergo auto-ubiquitination (**Fig. 2 A-C lane 8**). Addition of wild type USP28 to the enzyme assay was indeed able to reverse the auto-modification of DTX3L (**Fig. 2 A-C lane 9**) whereas $USP28^{C171A}$, a catalytically inactive mutant, was unable to do so (**Fig. 2 A-C lane 10**). The deubiquitination activity of USP28 did neither require the N-terminal region consisting of the ubiquitin-binding domains (UBA), the ubiquitin-interaction motif (UIM) and the SUMO-interaction motifs (SIM), nor the C-terminal extension as a fragment encompassing only the catalytic domain ($USP28^{cat}$, E147-L652) was sufficient to remove the ubiquitins from DTX3L (**Fig. 2 A-C lane 11**). Thus, these results show that USP28 can completely remove the ubiquitin modifications from DTX3L *in vitro*.

We next aimed to corroborate the results from the *in vitro* assay in cells. To this end, we performed DTX3L ubiquitination assays in HEK293 cells upon overexpression of DTX3L along with wild type USP28 and the catalytically inactive $USP28^{C171A}$ mutant. After DTX3L immunoprecipitation and western blot analysis with an ubiquitin antibody it was evident that overexpression of DTX3L alone increased the appearance of the polyubiquitin smear when compared to empty vector (Ctl) transfected cells (Fig. 2D); a finding in agreement with the autoubiquination of DTX3L in the in vitro assays. Furthermore, we found that wild type USP28 was able to reduce the appearance of the ubiquitin chains from DTX3L whereas the inactive mutant $USP28^{C171A}$ could not (**Fig. 2D**). Together, these data indicate that USP28 can act as a DUB on DTX3L.

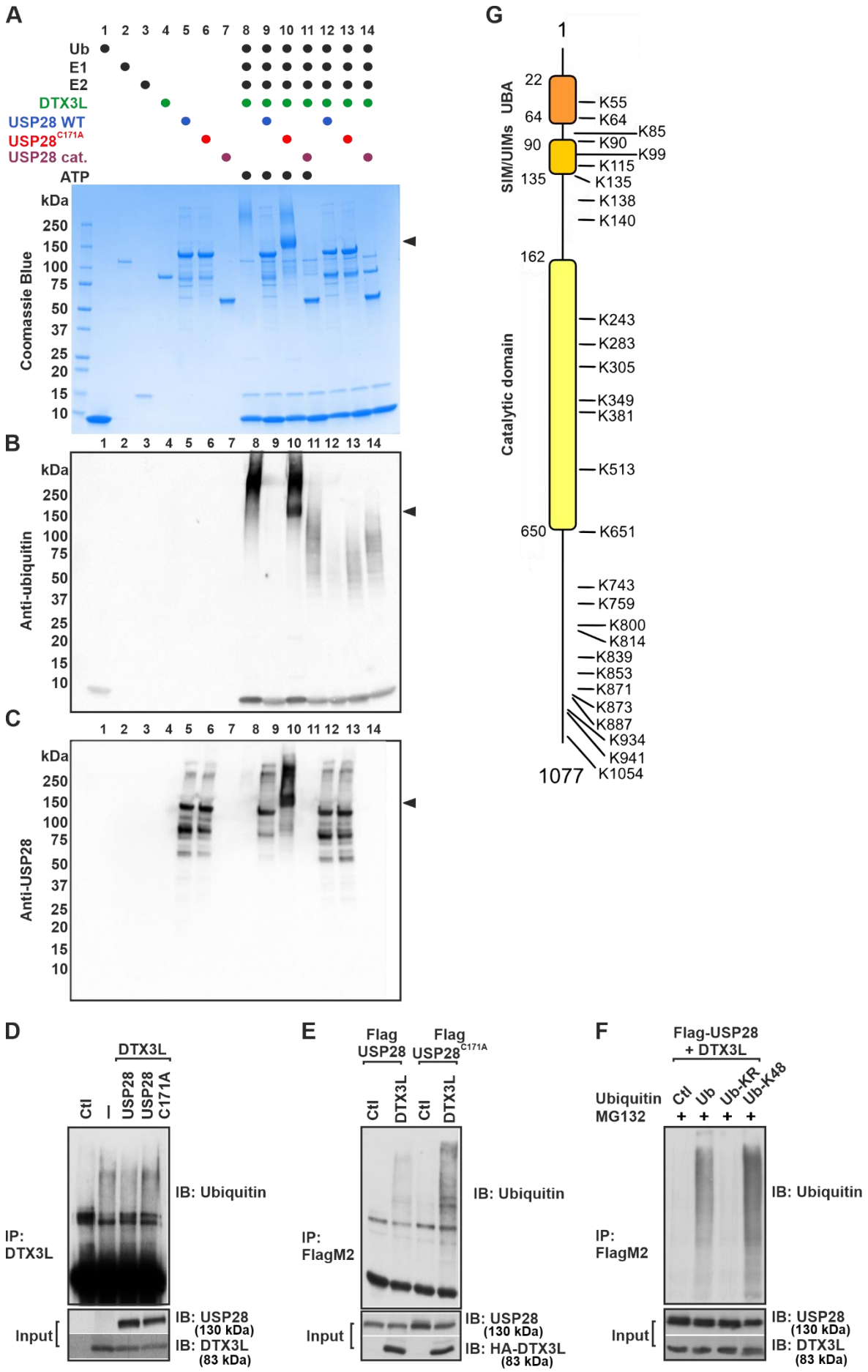
A
1 2 3 4 5 6 7 8 9 10 11 12 13 14
Ub
E1
E2
DTX3L
USP28 WT
USP28C171A
USP28 cat.
ATP
kDa
250
150
100
75
50
37
25
20
15
10
Coomassie Blue
B
Anti-ubiquitin
C
Anti-USP28
G
1
22
64
90
135
162
650
1077
UBA
SIM/UIMs
Catalytic domain
K55
K64
K85
K90
K99
K115
K135
K138
K140
K243
K283
K305
K349
K381
K513
K651
K743
K759
K800
K814
K839
K853
K871
K873
K887
K934
K941
K1054
D
DTX3L
Ctl
–
USP28
USP28 C171A
IP: DTX3L
IB: Ubiquitin
Input
IB: USP28 (130 kDa)
IB: DTX3L (83 kDa)
E
Flag USP28
Flag USP28C171A
Ctl
DTX3L
Ctl
DTX3L
IP: FlagM2
IB: Ubiquitin
Input
IB: USP28 (130 kDa)
IB: HA-DTX3L (83 kDa)
F
Flag-USP28 + DTX3L
Ubiquitin
MG132
Ctl
Ub
Ub-KR
Ub-K48
+ + + +
IP: FlagM2
IB: Ubiquitin
Input
IB: USP28 (130 kDa)
IB: DTX3L (83 kDa)

Figure 2. Functional interplay between USP28 and DTX3L. A) *In vitro* ubiquitination assay indicating the auto-ubiquitination activity of DTX3L and deubiquitinating activity of USP28. SDS-PAGE showing appearance of the DTXL3 ubiquitination pattern that is visible as a smear (lane 8) and its disappearance due to hydrolysis by USP28 (lane 9) and/or the USP28 catalytic domain (lane 11). Ubiquitinated DTX3L appears as a high molecular weight smear and the black arrow indicates a band that corresponds to ubiquitinated USP28. Note, that for unknown reasons USP28 preparations showed some degradation (lanes 5-6). B) Western blot of the assay in panel A probed with an anti-ubiquitin antibody. The black arrow indicates a band that corresponds to ubiquitinated USP28. C) Western blot of the assay in panel A probed with anti-USP28. The arrow indicates a band shift of the ubiquitinated catalytically inactive mutant USP28^{C171A} in the presence of ATP, Ubiquitin (Ub), E1 and E2 ligases as well as DTX3L. D, E, F) Cell based ubiquitination assays. HEK293 cells were transfected with an empty vector (Ctl) or expression vectors for DTX3L, wild type USP28 and the catalytically inactive mutant USP28^{C171A}. In D, ubiquitinated DTX3L was detected with ubiquitin antibody after immunoprecipitation of DTX3L. In E, ubiquitinated USP28 was detected with ubiquitin antibody after immunoprecipitation of USP28 with a FLAG-tag antibody. In F, cells were transfected with DTX3L and FLAG-USP28 expression vectors as well as with empty vector (Ctl) or vectors for wild type ubiquitin (Ubi), a mutant in which all lysine residues were converted to arginine (Ub-KR) or a mutant where only K48 remained intact (Ub-K48). Ubiquitinated USP28 was detected with ubiquitin antibody after immunoprecipitation of USP28 with a FLAG-tag antibody. G) Domain organization of USP28 and the ubiquitination sites identified by mass spectrometry using the USP28^{C171A} mutant. UBA, - ubiquitin-associated domain; UIM, -ubiquitin interaction motif; SIM,- SUMO interaction motif.

DTX3L ubiquitinates USP28

In addition to the auto-ubiquitination of DTX3L, we also observed that DTX3L could ubiquitinate the USP28^{C171A} mutant (**Fig. 2A lane 10**). This was only seen with the inactive USP28^{C171A} mutant because the active USP28 would deubiquitinate itself as well as DTX3L (**Fig. 2A lane 9**). When membranes were probed with an anti-ubiquitin antibody, the modified USP28^{C171A} became visible as a band that migrates faster in comparison to auto-ubiquitinated DTX3L and represents modified USP28^{C171A} (**Fig. 2B lane 10, black arrow**). To further confirm this, we probed the membrane with an anti-USP28 antibody. As expected, the blots reveal a shift of the band representing USP28^{C171A} towards a higher molecular weight as result of the ubiquitination (**Fig. 2C lane 10 versus lane 6**). Similarly, when we performed ubiquitination assays for USP28 in cells that either overexpressed wild type USP28 or the inactive USP28^{C171A} along with DTX3L, we found that DTX3L promoted ubiquitination of USP28. In line with the *in vitro* ubiquitination assay, this was especially evident in the cells expressing USP28^{C171A} (**Fig. 2E**). To further investigate whether the ubiquitination of USP28 by DTX3L renders it susceptible for proteasomal degradation, we performed an additional ubiquitination assay in the presence of either wild type ubiquitin or two specific ubiquitin mutants. In the first mutant, all lysine residues were converted to arginine (Ub-KR), preventing ubiquitination and, in particular, polyubiquitin chain formation. As expected, use of this mutant resulted in loss of USP28 ubiquitination by DTX3L (Fig. 2F). In the second mutant (Ub-K48),

only one lysine, *i.e.*, K48, remained intact. Therefore, only K48-linked polyubiquitin chains can be formed when this mutant is used. The assay shows that DTX3L is able to ubiquitinate USP28 in the presence of this mutant. Given that such K48-linked polyubiquitin chains are known to target proteins for degradation by the proteasome, these data indicate that the formation of K48-polyubiquitin chains on USP28 by DTX3L target USP28 for proteasomal degradation (Fig. 2F).

Next, we used mass spectrometry to identify the sites within $USP28^{C171A}$ that become ubiquitinated in the presence of DTX3L. In total, 28 lysines were found to be modified by DTX3L and those ubiquitination sites were distributed over the whole protein without any domain preference (**Fig. 2 F,G)**. Together, the data show that USP28 can act as a DUB on DTX3L and vice versa, that USP28 is a substrate for DTX3L.

DTX3L and USP28 mutually control their levels in cells

DTX3L is known to function as an E3 ubiquitin ligase, promoting the ubiquitination and subsequent degradation of interacting target proteins such as USP28. On the other hand, as a deubiquitinase USP28 can remove ubiquitin modifications leading to their stabilization. As the in vitro studies have shown that both, DTX3L and USP28, appear to control each other's ubiquitination, we next aimed to investigate whether this mutual interplay affects their stability in a broader physiological context in cells.

First, we wanted to test if DTX3L would regulate USP28 levels and vice versa whether USP28 would regulate DTX3L levels. To this end, we first overexpressed DTX3L in SK-MES-1 lung tumor cells and analyzed USP28 levels. As USP28 plays a role in various stress pathways including hypoxia signaling. (18) we also exposed those cells to normoxia and hypoxia in order to examine changes in downstream USP28 substrates such as HIF-1α, p53, and c-MYC (19). When analyzing the cells, we observed that overexpression of DTX3L decreased USP28 levels under both normoxia and hypoxia (**Fig. 3A**) which is in agreement with polyubiquitination of USP28 by DTX3L. In line with previous observations the decrease of USP28 was accompanied by a reduction in HIF-1α (18), p53 (20), and c-MYC levels. (13, 16, 20, 21) (22) Knockdown of DTX3L using two different DTX3L shRNAs raised USP28 protein levels up to two-fold and induced HIF-1α levels under hypoxia, and p53, and c-MYC levels under both normoxia and hypoxia (**Fig. 3A,B**).

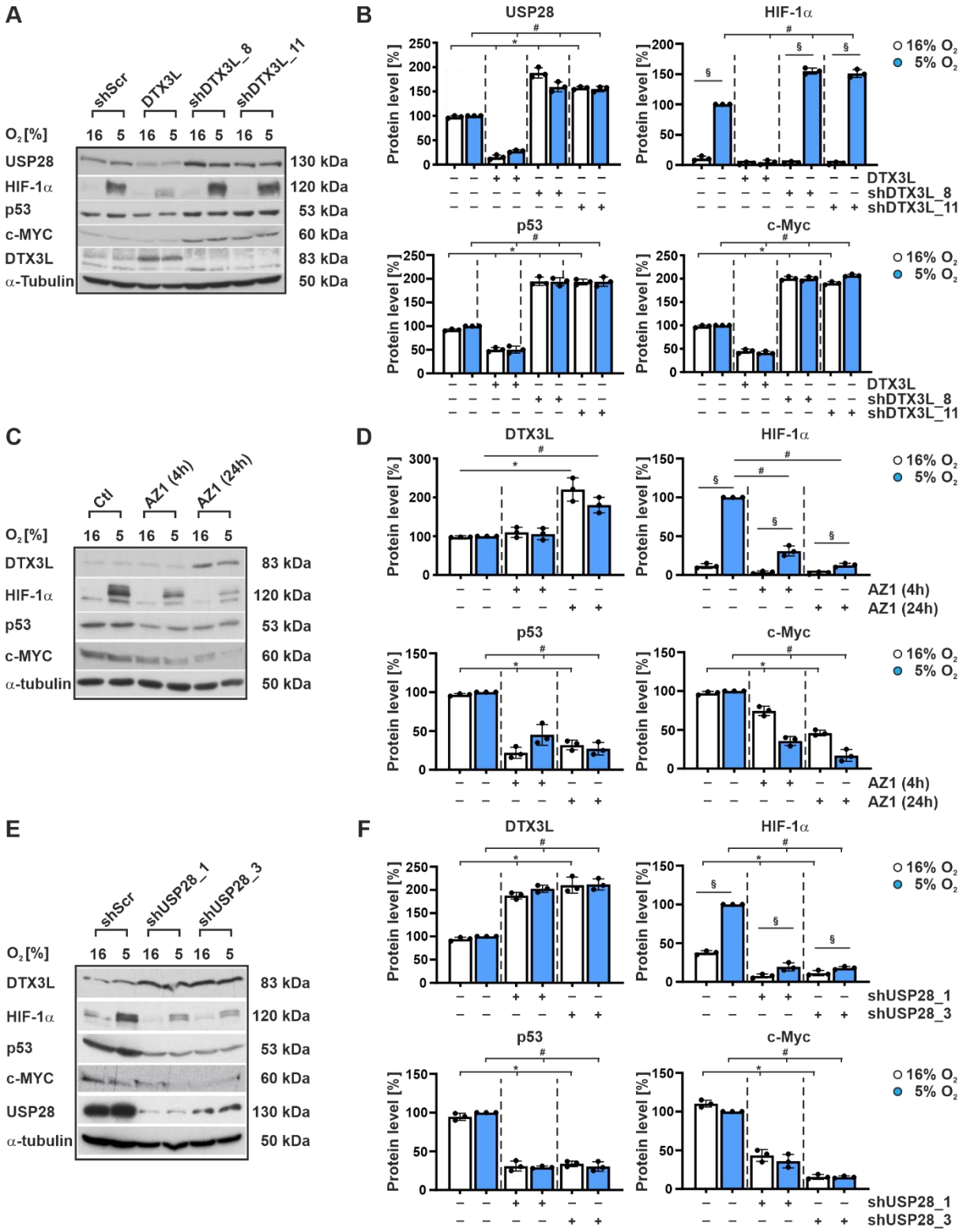

Figure 3. Mutual regulation of DTX3L and USP28 protein levels. A) SK-MES-1 cells were transfected either with expression vector for scrambled control shRNA (shScr), or with expression vectors for full-length DTX3L or one of two independent shRNAs (shDTX3L_8, shDTX3L_11) against DTX3L. After transfection, cells were further cultured under normoxia (16% O_2) or hypoxia (5% O_2) for 4 hours. USP28, HIF-1α, p53, c-MYC, and DTX3L protein levels were measured by Western blot analysis. Alpha tubulin served as a loading control. B)

Quantification of USP28, HIF-1α, p53 and c-MYC. C) SK-MES-1 cells were treated with the USP28/25 inhibitor AZ1 (10 µM) and cultured under normoxia and hypoxia for 4 h and 24 h. DTX3L, HIF-1α, p53, and c-MYC protein levels were measured by Western blot analysis. D) Quantification of DTX3L, HIF-1α, p53 and c-MYC. E) SK-MES-1 cells were transfected with expression vectors for scrambled control shRNA (shScr) or shRNA 1 or shRNA 3 against USP28. After transfection, cells were further cultured under normoxia or hypoxia for 4 h. DTX3L, HIF-1α, p53, c-Myc and USP28 protein levels were measured by Western blot analysis. F) Quantification of DTX3L, HIF-1α, p53 and c-MYC. In each experiment the protein levels at 5% O_2 control (Ctl) or shScr were set to 100%. *significant difference for 16% O_2: Ctl vs DTX3L, vs shDTX3L, vs shUSP28 or vs AZ1 , §significant difference between 16% O_2 vs 5% O_2, $^{\#}$significant difference for 5% O_2: Ctl vs DTX3L, vs shDTX3L, vs shUSP28 or vs AZ1, $p < 0.05$, $n = 3$.

Next, we were interested to see the impact of USP28 on DTX3L. As USP28 can remove the auto-ubiquitination from DTX3L, it would at first glance be expected that inhibition or lack of USP28 would reduce DTX3L levels due to enhanced degradation. We tested this assumption by using two approaches. Firstly, we exposed cells to the dual selective USP28/25 inhibitor AZ1 (23) and secondly, we used two different shRNAs targeting USP28 (18). In contrast to our hypothesis, we found that both chemical as well as genetic inhibition of USP28 upregulated the levels of DTX3L whereas HIF-1α, p53, and c-MYC were downregulated (**Fig. 3C-F**).

As coupled changes in ubiquitination and protein amount are commonly the result of a changed half-life we next measured whether DTX3L and USP28 could influence each other´s protein half-life after depletion of the one or the other with specific shRNAs in HEK293 cells. On the one hand, we found that the half-life of both DTX3L and USP28 is about 5 h when cells are transfected with scrambled shRNA **(Fig. 4A,C)**. As before, knockdown of DTX3L led to an increase in USP28 levels at time point zero of the cycloheximide challenge and further to an at least two-fold increase in USP28´s half-life (**Fig. 4A,B**). On the other hand, we again observed that depletion of USP28 resulted in an increase of DTX3L levels at time zero and further also in an increase in it´s half-life **(Fig. 4C,D)**. Similarly, depletion of USP28 in breast cancer cells (MDA-MB237) also increased DTX3L´s half-life whereas overexpression of USP28 shortened the DTX3L half-life (**Fig. S4**). Altogether, the current findings show that the E3 ligase DTX3L and the DUB USP28 can mutually reduce each other´s half-life.

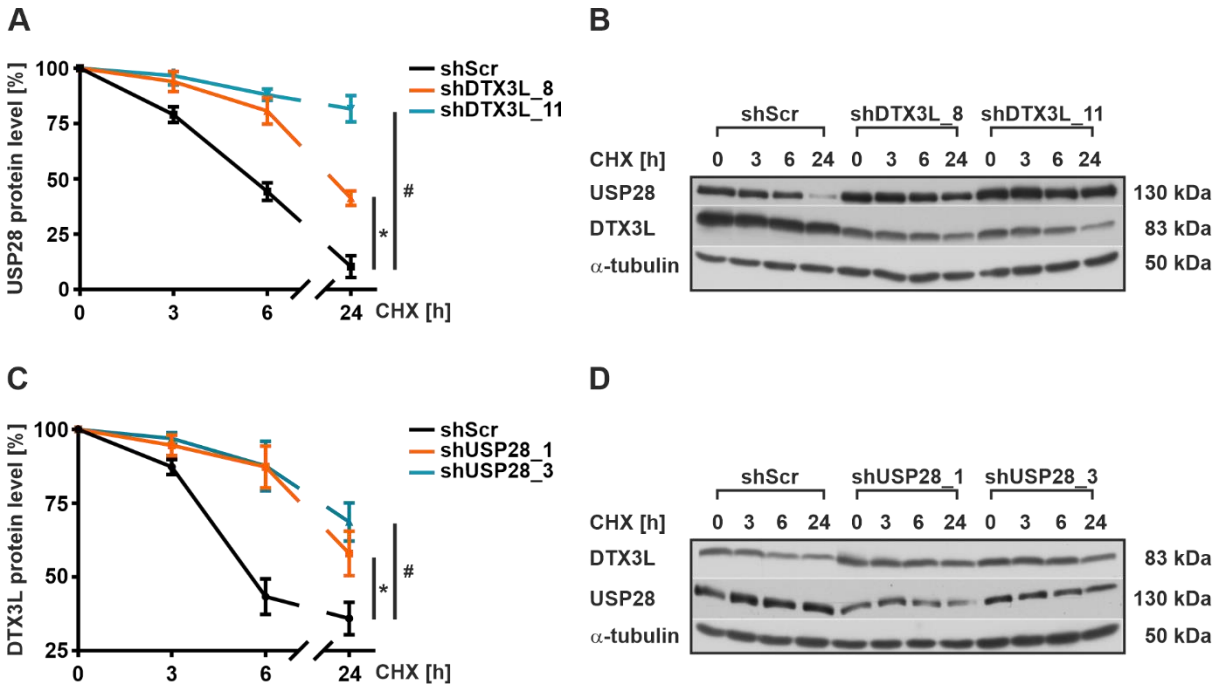

Figure 4. DTX3L and USP28 control each other´s half-life. (A,C) HEK293 cells were transfected with scrambled shRNA or with two different shRNA´s against either DTX3L or USP28. After transfection, protein synthesis was inhibited with cycloheximide (CHX; 10 µg/µl) and cells were harvested at indicated time points. In each experiment the protein levels at time point 0 were set to 100%. *significant differences shScr vs shDTX3L or shUSP28_1, #significant differences shScr vs shDTX3L_11 or shUSP28_3, $p \leq 0.05$, n=3. (B,D) Representative Western blot analysis. 100 µg of total protein lysate was analyzed with antibodies against USP28, DTX3L and α-tubulin.

DTX3L and USP28 control DNA repair pathways

The most critical DNA lesions are double-strand-breaks (DSB). Several pathways are available to repair these detrimental lesions in cells. These include non-homologous end joining (NHEJ), homologous recombination (HR), single-strand annealing (SSA), and microhomology-mediated end joining (MMEJ). Canonical NHEJ directly joins both ends of the DSBs and is only partially error free (24), as a few nucleotide insertions or deletions may occur due to minor end processing. For comparison, HR uses homologous sequences of the sister chromatid as template and is therefore considered error-free. SSA is another example of homologous repair but requires extensive processing of the broken DNA ends before annealing between single stranded DNA repeats, resulting in deletions and therefore loss of genome integrity (25). MMEJ is different from SSA as it uses only microhomologies of a few base pairs between the two strands that arise after resection of the broken ends. As a consequence, MMEJ is always error-prone (26).

To analyze a potential participation of DTX3L and USP28 in DSB repair we used an established EGFP-based reporter system allowing measurements of NHEJ, MMEJ, and both

conservative HR and non-conservative SSA following I-*Sce*I meganuclease-mediated DNA cleavage (27–29).

First, we engaged substrate EJ5SceGFP, which monitors all NHEJ events, that is, both simple rejoining between two cleaved I-*Sce*I sites as well as error-prone events accompanied by deletion or insertion of nucleotides (29). The results revealed that NHEJ frequencies were not affected when comparing MDA-MB237 control with USP28 KD cells or cells with knockdown of DTX3L. However, NHEJ frequencies decreased by about 30% upon combined knockdown of USP28 and DTX3L **(Fig. 5A, B).**

Next, we focused on HR using the substrate HR-EGFP/5′EGFP, and found that HR frequencies decreased by about 40% upon combined knockdown of USP28 and DTX3L compared to empty vector control, but also compared to single knockdown samples **(Fig. 5C, D)**. Similar effects were noted when assessing SSA frequencies after double knockdown **(Fig. 5E, F)**. Further, single knockdown of DTX3L decreased SSA frequencies compared with single USP28 knockdown.

When we next assessed error-prone MMEJ by use of EJ-EGFP (27) we found that knockdown of USP28 decreased MMEJ frequencies by about 70%. Interestingly, knockdown of DTX3L alone did not affect MMEJ frequencies whereas knockdown of both DTX3L and USP28 decreased MMEJ by 25% only; hence, knockdown of DTX3L partially antagonized the USP28-mediated effects on MMEJ **(Fig. 5G, H)**. Thus, these data indicate that the regulatory interplay between DTX3L and USP28 modulates each DSB repair activity, whereby the impact on MMEJ differs from the one on all other pathways.

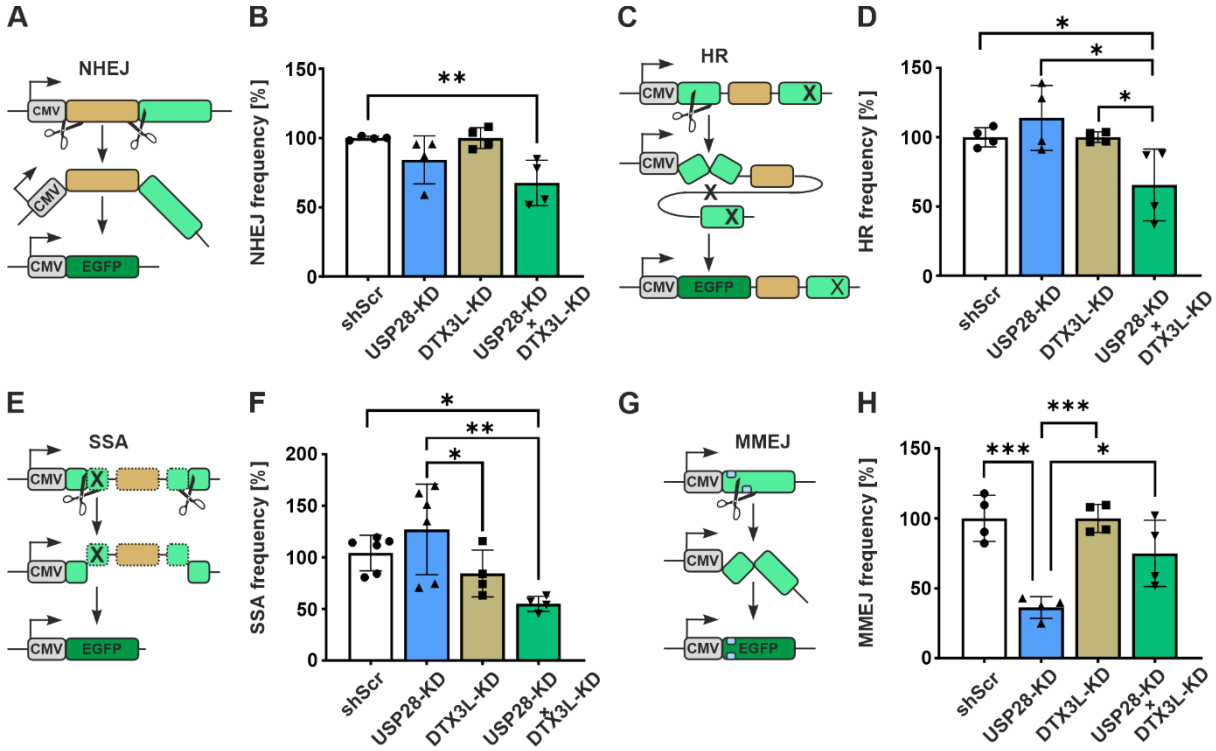

Figure 5. DSB repair analysis. Pathway-specific repair activities were measured in cells using EGFP reporter assay. MDA-MB237 Scr, and USP28 KD1 cells transfected with shRNAs against DTX3L or empty vector were cultured for 24 h prior to nucleofection with a DNA mixture consisting of I-*Sce*I meganuclease expression plasmid pCMV-I-Sce-I, balancing plasmid pBS (determination of repair frequency) or wild-type EGFP expression plasmid (determination of transfection efficiency), and DSB repair substrate to evaluate NHEJ (A,B), HR(C,D), SSA (E,F) or MMEJ (G, H). Percentages of EGFP-positive cells were measured 48 h later and normalized to the individually determined transfection efficiencies to allow calculation of DSB repair frequencies. Mean values for the MDA-MB237 Scr cells (shScr) were defined as 100%. Data are mean +/- SD from 4-6 measurements. The statistical significance of differences was determined using ordinary one way ANOVA. *P<0.05, **P<0.01 ***P<0.001.

Discussion

The current study is the first one providing evidence for an interplay between the E3 ubiquitin ligase DTX3L and the DUB USP28. The findings present novelty in several aspects. First, the interplay between the two proteins is based on a direct physical transient interaction; second, they regulate each other's levels in a mutual manner; and third, the reciprocal regulation affects USP28 target proteins and the cellular DSB repair capacity. These studies on the DTX3L–USP28 interaction suggest synergistic roles in DNA damage repair and cancer biology.

DTX3L was originally identified as a binding partner of PARP9, which is an oncogenic factor in diffuse large B-cell lymphoma (DLBCL) (30). Interestingly, those former studies indicated that DTX3L shuttles between the cytoplasm and the nucleus, and proposed that DTX3L may target specific proteins within the nucleus. Although neither the former nor the current study analyzed the nuclear shuttling process per se, we also observed that DTX3L can localize to both the cytoplasm and the nuclear compartments which supports the notion that nuclear proteins might be DTX3L targets. Indeed, in our work HIF-1α, p53, and cMYC levels, all nuclear based transcription factors, were found to be decreased upon forced expression of DTX3L. Our finding that USP28 preferentially localizes to the nucleus is also in line with earlier reports (13) and indicates that its antagonistic action on DTX3L is very likely a nuclear event, although DTX3L has roles both in the nucleus and the cytoplasm (8, 31). In addition, we show that HIF-1α, p53 and c-MYC protein levels are reduced in the absence of USP28.

Preceding studies indicated that DTX3L is abundant at DNA lesion sites suggesting that it might be involved in the ADP-ribosylation dependent DNA damage response (32, 33). More specifically, DTX3L in complex with PARP9 was shown to be recruited to sites of DNA damage by PARP1 (7). Different from PARP1, PARP9 was first described as a catalytically inactive member of the ARTD family (34, 35) and more recently found to form a complex with DTX3L and regulate mono-ADP-ribosylation and E3 Ub ligase functions of DTX3L (5, 6, 36). Simultaneously, PARP9 recognizes ADP-ribosylated proteins and therefore recruits the complexed E3 ligase to its substrate for ubiquitination and ultimately degradation (37). Given that recruitment of USP28 to DSBs by TP53BP1 was previously found to be enhanced by PARP9 in complex with DTX3L (4), we examined the functional impact of such a colocalization of the Ub E3 ligase and the DUB. We purified full-length DTX3L and USP28 as well as its catalytically inactive mutant and studied ubiquitination in vitro and via immunoprecipitation in cellulo. These analyses demonstrated that DTX3L can ubiquitinate itself and that USP28 can remove the ubiquitin chains from DTX3L, which relied on the comparison of catalytically active (full-length USP28, catalytic domain of USP28) and inactive ($USP28^{C171A}$) versions of USP28. Ablation of the DUB activity in $USP28^{C171A}$ enabled us to demonstrate that also USP28 represents an ubiquitination substrate of DTX3L. Our MST measurements identified a wide distribution of Ub modified lysines along the USP28 molecule. Interestingly, K64, 85, 99, 115, and 135 were previously identified as sumoylation sites using an *in vitro* assay (38), and among these lysines, K99 was shown to be most efficiently sumoylated compared to others. These sumoylated and ubiquitinated amino acids reside within the N-terminus comprising the UBA domain and the SIM/UIMs. SUMO modifications in these regions negatively regulate USP28 catalytic activity (38) and our results indicate that there could be a dynamic regulation of USP28 through competition between sumoylation and ubiquitination. All in all, these experiments revealed physical and functional interactions between DTX3L and USP28 assembling Ub E3 ligase and DUB activities, respectively, directed towards both enzyme components of the heterodimeric complex and to downstream proteins involved in signaling different types of stress such as hypoxia or DNA damage.

DTX3L in complex with PARP9 was previously suggested to be involved in DNA repair, as deletion of either gene increased the cellular sensitivity to DNA damaging agents (36). USP28 physically interacts with and regulates several DSB repair factors (16, 17, 39, 40). Our

systematic analysis of specific DSB repair pathways revealed synthetic dysfunction in NHEJ, HR and SSA after combined but not after individual knockdown of DTX3L or USP28. These results suggested synergy between these two players in the ubiquitin-mediated regulation of the DNA damage response. To the contrary, when focusing on MMEJ, single knockdown of USP28 compromised this error-prone DSB repair activity, whereas additional knockdown of DTX3L rescued MMEJ repair activity. From this, we conclude that MMEJ depends on USP28´s DUB activity as long as the Ub E3 ligase DTX3L is active. Of note, NBS1, a component of the MRE11-RAD50-NBS1 (MRN) complex is a key player in MMEJ (41). NBS1 is a DUB substrate and subject to positive regulation by USP28 (40), so that it is very likely that initial end processing by MRN contributes to the USP28-mediated effect on MMEJ.

Different from the antagonism of USP28 and DTX3L in MMEJ, synergistic effects on the other DSB repair pathways must be explained by complementary activities of the two enzymes. Of interest, DTX3L-mediated histone ubiquitination was reported to promote recruitment of the key DSB repair players TP53BP1, RAP80, and BRCA1 to DNA damage sites (7, 36). Here, we demonstrated physical and functional interactions between DTX3L and USP28 and confirmed that USP28 interacts with the end-binding protein TP53BP1, which is known to be stabilized by USP28 (13). T53BP1 represents a platform to assemble USP28 together with its DUB substrates like p53 that favors NHEJ at the expense of error-prone MMEJ (17, 27, 42, 43). TP53BP1 itself ensures canonical NHEJ between proximal DNA ends (44, 45), so that these DTX3L- and USP28-dependent actions on TP53BP1 may underlie the observed synthetic NHEJ defect after double knockdown. Differently, but in agreement with previous work (12), single USP28 knockdown did not cause a significant change of NHEJ, HR and SSA in our measurements. Single DTX3L knockdown also did not affect DSB repair except for a decrease of SSA when compared with USP28 knockdown. Though a specific role of DTX3L (and USP28) in the pathway of SSA has not been studied before, such deleterious events may have contributed to the deleterious NHEJ activities that were previously found to be reduced already after single DTX3L knockdown (36). Both SSA and HR rely on efficient end processing by the MRN and BRCA1/CtIP complexes in concert with the regulatory kinase CHK2 (46). Accordingly, we suggest that combined downregulation of DTX3L and USP28 severely compromise these pathways through inefficient BRCA1 recruitment (7) and reduced stability of NBS1, CHK2 as well as other checkpoint factors (13), respectively. Aside from such direct activities on DNA damage response factors, USP28 also activates NFκB signaling (39), which transcriptionally upregulates the NHEJ protein Ku70, the HR factors ATM and BRCA2 and activates BRCA1/CtIP (47–50).

Altogether, DTX3L and USP28 show complementary modes-of-action in promoting NHEJ and homologous DSB repair (SSA and HR), namely via recruitment and accumulation of enzymatic and regulatory DSB repair components, respectively. In this work, we also provide insight into the molecular details of this cooperation. We provide evidence for physical and functional interactions between DTX3L and USP28 catalyzing ubiquitination and deubiquitination processes directed towards each other and towards downstream DNA damage response factors. DTX3L and USP28 share common substrates ranging from hypoxia-inducible HIF-1α with relevance for anti-cancer treatment and immune responses (51), to c-MYC, more recently seen

in protecting against transcription-coupled replication stress (52). All in all, DTX3L and USP28 interaction may represent rheostats that more generally fine-tune cellular stress responses with a pro-survival or pro-apoptotic outcome depending on the context.

Experimental Procedures

Production of recombinant proteins

A codon optimised DNA encoding human USP28 was procured from Genscript and cloned between the NdeI/BamHI multiple cloning site (MCS) of pMJS162 (53). The expression vector for USP28 was then transformed into MDS42 bacterial cells and a starter culture was prepared in 5 ml of LB medium (Formedium, UK) with carbenicillin (100 µg/ml). After 14 h of incubation at 37°C, the starter culture was used to inoculate 500 mL of Terrific Broth (TB) autoinduction media with trace elements (Formedium,UK) supplemented with glycerol [0.8 (w/v)] and carbenicillin (100 µg/ml). Cultures were incubated briefly at 37°C until they reached and OD_{600} of 1.0, after which the temperature was decreased to 15°C for overnight incubation. Cells were harvested by centrifugation at 4200xg for 45 min at 4°C and re-suspended in lysis buffer [50 mM HEPES (pH 7.5), 500 mM NaCl, 0.5 mM TCEP, 10% (v/v) glycerol, 10 mM imidazole]. Re-suspended pellets were flash frozen in liquid N_2 and stored at -20°C until purification.

To purify USP28, cell pellets were sonicated and centrifuged at 27,600×g to resuspend soluble protein. The soluble fraction was filtered through a 0.45 µm sterile syringe filter and loaded onto a pre-equilibrated 5 mL HiTrap IMAC HP column (GE Healthcare Biosciences). The column was washed with 4 column volumes of lysis buffer followed by 4 column volumes of wash buffer 1 [50 mM HEPES (pH 7.5), 500 mM NaCl, 10% (v/v) glycerol, 0.5 mM TCEP, 50 mM imidazole]. To remove chaperone proteins, the column was washed with 4 column volumes of wash buffer 2 [50 mM HEPES (pH 7.5), 150 mM NaCl, 10% (v/v) glycerol, 10 mM imidazole, 0.5 mM TCEP, 5 mM ATP, 1 mM $MgCl_2$]. Protein was recovered through a gradient elution from 10 mM imidazole to 500 mM imidazole. Pooled fractions from the elution were run through Superdex S200 16/600 gel filtration column for further purification. Protein fractions were verified by SDS-PAGE and pooled, concentrated, flash frozen with liquid N_2 and stored at –70°C.

DTX3L and other proteins used for ubiquitination reactions were purified as described previously (6). Nucleic acid contamination was assessed using absorbance ratio of 260 nm over 280 nm for DTX3L (0.7) and USP28 (0.5).

In vitro ubiquitination assays

Typically, 50 µl ubiquitination reactions were performed. Proteins were diluted in 50 mM Hepes pH 7.5, 50 mM NaCl. Protein concentrations used were Ub (50 µM), E1 (0.4 µM), UbcH5a (E2) (2 µM) and DTX3L (0.7 µM). USP28 was used at a final concentration of 3 µM. Reactions were assembled on ice and then initiated by addition of ubiquitination buffer (20X

concentration: 1M tris pH 7.5, 40 mM ATP, 100 mM MgCl2, 40 mM DTT) to a final concentration of 1X and incubated at room temperature for 2-3 h. Outcomes of the reactions were analyzed by SDS-PAGE Coomassie blue staining or by Western blotting. Ubiquitination sites in $USP28^{C171A}$ were identified as described in (6).

Microscale thermophoresis (MST)

The dissociation constant (K_d) between DTX3L and USP28 was measured with Monolith (NanoTemper) using a RED-NHS 2ndgeneration labeling dye (NanoTemper). NHS ester groups covalently crosslink lysine residues. DTX3L was labeled by adding 30 µM dye to 10 µM protein, 100 µl of ligand buffer [20 mM HEPES (pH 7.4), 350 mM NaCl, 0.5 mM TCEP]. The labeling reaction was incubated for 60 min at room temperature, in the dark, and excess dye was removed with a desalting column pre-equilibrated with 12 ml of ligand buffer. Labeled protein was recovered in 450 µL of ligand buffer. The degree of labeling was determined to be 90% based on the absorbances at 280 nm and 650 nm.

For affinity measurements, labelled DTX3L (20 nM final concentration) was added to a serial dilution of USP28 (22.5 µM to 0.68 nM). Immediately after mixing, 10 µl were loaded onto the Monolith NT.115 Premium Capillaries (NanoTemper). The MST signal was recorded with NT.Control v2.1.31 software and data was fitted to a K_d model with MO.Affinity Analysis v2.3 software.

Cell cultures

SK-MES1 and human embryonic kidney 293 (HEK 293) cells were cultured under normoxia (16% O_2, 79% N_2 and 5% CO_2 [by volume]) in minimal essential medium (MEM) supplemented with 10% fetal bovine serum (FBS). MDA-MB 231 cells with stable USP28 knockdown were generated as described (20) and cultured in DMEM supplemented with 10% FBS.

All cell lines were tested Mycoplasma negative by using the MycoAlert Detection Kit (Lonza). In all experiments the number of cell passages used was below 10. For protein extraction, cells were seeded onto 6 cm dishes. After a medium change, cells were treated with the USP25/28 inhibitor AZ1 (10 µM), further cultured for 24 hours either under normoxia or hypoxia (5% O_2, 90% N_2, and 5% CO_2) and then harvested. In all experiments control cells were treated with DMSO.

Plasmid constructs for knockdown and protein expression

The constructs for pDZ-Flag-USP28, pRetrosuper-USP28 shRNA-1, and pRetrosuper- USP28 shRNA-3 were described previously (18). The full length USP28 construct with mutation in

cysteine 171 was generated using the QuickChange mutagenesis kit (Promega) as described (18).

The constructs for pLKO.1-shDTX3L_8 (TRCN0000073208) and pLKO.1-shDTX3L_11 (TRCN0000073211) were from Sigma Aldrich MISSION shRNA library, distributed by Genome Biology Unit core facility supported by HiLIFE and the Faculty of Medicine, University of Helsinki, and Biocenter Finland.

The constructs for pRK5-HA-Ubiquitin-WT (Addgene plasmid #17608), pRK5-HA-Ubiquitin-KO (Addgene plasmid #17603) and pRK5-HA-Ubiquitin-K48 (Addgene plasmid #17605) were a kind gift from Ted Dawson and described previously (54).

Western blot analysis, protein half-life studies and co-immunoprecipitation.

Western blot analysis was carried out as described previously (55). In brief, purified proteins or total mammalian cell lysates were separated by sodium dodecyl sulfate (SDS)-polyacrylamide gel electrophoresis. After electrophoresis and electroblotting onto a nitrocellulose membrane, membranes were blocked at room temperature for 1 h with 1X casein blocking solution (Bio-Rad) (#1610782). Proteins were detected with monoclonal antibodies against ubiquitin (BioLegend Cat. No. 646304; 1:1000), human HIF-1α (#610959; 1:1000; BD Bioscience), p53 (#48818; 1:1000; Cell signaling), DTX3L (#HPA010570; 1:1000; Sigma-Aldrich), HA-Tag (F-7) (#sc7392; 1:1000; Santa Cruz), and against α-tubulin (clone B-5-1-2) (#T5168; 1:10.000; Sigma-Aldrich). Polyclonal antibodies in this study were used against USP28 (#HPA006778; 1:1000; Sigma-Aldrich), TP53BP1 (#NB100-304; Novus Biologicals) and c-MYC (C-19) (#sc-788; 1:500; Santa Cruz). The secondary antibodies were either anti-mouse (#1706516; 1:5000; Bio-Rad)- horseradish peroxidase, anti-mouse (Dako P044701-2; 1:1000) Alexa Fluor 488 or anti-rabbit (#1706515; 1:5000; Bio-Rad) horseradish peroxidase conjugated immunoglobulin G, engaged in the ECL system (GE Healthcare, Germany).

For half-life studies, HEK 293 cells were transfected with expression vectors encoding full length USP28, USP28^{C171A} or full length DTX3L. After 24 h, cycloheximide (10 µg/ml; Sigma-Aldrich) was added to the medium, cells were harvested at the indicated time points and protein levels were measured by immunoblot analysis.

For co-immunoprecipitation, the cells were pretreated with the proteasome inhibitor MG 132 (50 µM; Calbiochem) for 4 h. Cells were washed twice with ice-cold 1x PBS, then (dithiobis(succinimidyl propionate)) DSP was added to a final concentration of 2 mM and cells incubated for 2 h at 4°C. To terminate the reaction, glycine was added to a final concentration of 10 mM for additional 15 minutes. Then cells were scraped in lysis buffer (50 mM Tris/HCl, pH 7.5, 150 mM NaCl, 1% Triton X-100, 2 mM EDTA, 2 mM EGTA, 1 mM PMSF, and complete protease inhibitor cocktail tablet; Roche), incubated with continuous shaking at 4°C for 20 min and then centrifuged at 12 000xg at 4°C for 15 min. To recover immunoprecipitates, 150 µg of protein lysate was incubated with 2 µg of antibodies against TP53BP1, USP28, DTX3L and Flag epitope for 1 h at 4°C before Protein G Sepharose beads (30 µL per reaction mixture; GE Healthcare #GE17-0618-01) were added for 12 h. Thereafter, the beads were washed 5 times with lysis buffer and recovered, pellets were dissolved in 2x Laemmli buffer,

loaded onto a 7.5% SDS gel, blotted, and detected with Abs against DTX3L, USP28 and ubiquitin.

Immunofluorescence

MDA-MB 231 cells were grown on coverslips. When cells reached sufficient confluency, media was removed, cells were washed with PBS and fixed in 4% paraformaldehyde for 10 min and washed with PBS. Blocking was performed in PBS containing 5% fetal bovine and 5% goat serum for 1 h. This was followed by incubation with primary antibodies against DTX3L (Santa Cruz Biotechnology, Inc) and USP28 (Sigma-Aldrich); both were diluted in 1% blocking buffer and incubated with the coverslips overnight at 4 °C. After overnight incubation samples were washed in PBS and incubated with Alexa Fluor anti-mouse 488 and anti-rabbit 546 secondary antibodies (Invitrogen) diluted in 1% blocking buffer at room temperature for 1 h, respectively. Cell nuclei were visualized by Hoechst 33342 staining (Invitrogen). The specimens were mounted with Immu-Mount (Fisher Scientific) and fluorescent images were obtained by confocal microscopy (LSM700, Zeiss).

DSB repair

Analysis of DSB repair was conducted as described (27, 29, 56). In brief, plasmid constructs expressing the endonuclease I-*Sce*I (pCMV-I-SceI) and reporter constructs encoding different DSB repair substrates for NHEJ (EJ5SceGFP), MMEJ (EJ-EGFP), homologous recombination, HR (HR-EGFP/5´EGFP), and SSA (5´EGFP/HR-EGFP) were introduced by nucleofection according to the Amaxa protocol (Lonza, Cologne, Germany). To balance the DNA amount and to control transfection efficiencies, transfection mixtures for split cell culture samples contained either pBlueScriptII KS (pBS, Stratagene, Heidelberg, Germany) or wild-type EGFP expression plasmid, respectively. Mean transfection efficiencies were in the range of 50%. After transfection, cells were further cultured for another 48 h. Thereafter, DSB repair was monitored via quantification of EGFP-positive cell fractions with a LSR Fortessa (Becton Dickinson) flow cytometer and analyzed by the diagonal gating method in the Fl1/Fl2 dot plot as described (27) by using the FlowJo 10.7.1. program. Each quantification of green fluorescent cells in repair assays was normalized by use of the individually determined transfection efficiency to calculate the DSB repair frequency.

Statistical Analysis

Densitometry data were plotted as fold induction of relative density units, with the zero-value absorbance in each figure set arbitrarily to 1 or 100%. If not otherwise stated statistical comparisons of absorbance differences were performed by the Mann-Whitney test (Statview 4.5, Abacus Concepts, Berkeley, CA), and p values $p < 0.05$ were considered significant.

Data availability

Data are contained within the manuscript and the provided supporting information.

Supporting information

This article contains supporting information.

Acknowledgements

We thank Philomena Schmid, Célia Tebbakh and Sabrina Arnold for technical assistance. The authors are grateful to Virpi Glumoff for FACS sorting with DNA repair GFP constructs. The use of the facilities and expertise of the Biocenter Oulu Structural Biology core facility (a member of Biocenter Finland, Instruct-ERIC Centre Finland and FINStruct), Proteomics and Protein Analysis core facility (a member of Biocenter Finland) and Biocenter Oulu sequencing center are gratefully acknowledged. MST experiments were carried out in the FINStruct site at the University of Helsinki. AZ1 was a generous gift from David M Andrews (AstraZeneca).

Author contributions

Y.A., L.L, T.K. conceptualization; Y.A, D.M., C.V.-R., H.I.A. and R.P.-H. investigation; M.R.-S and L.W. methodology; Y.A, D.M., C.V.-R., L.L., L.W. and T.K. writing-original draft; Y.A, D.M. C.V.-R., R.P.-R., M.R-S., L.W., L.L. and T.K. writing-reviewing and editing; L.L. and T.K. funding acquisition; R.P.-H., L.L. and T.K. supervision.

Funding

We acknowledge funding from Biocenter Oulu spearhead projects (LL and TK), Jane and Aatos Erkko Foundation (LL and TK), Academy of Finland Profi6 (336449) and Sigrid Jusélius Foundation (to RPH) as well as from the German Research Foundation (DFG) Project B3 in the Collaborative Research Center 1506 "Aging at Interfaces" to M.R.-S. and L.W.

Conflict of interest

The authors declare that they have no conflicts of interest with the contents of this article.

References

1. Mennerich, D., Kubaichuk, K., and Kietzmann, T. (2019) DUBs, Hypoxia, and Cancer. *Trends Cancer*. **5**, 632–653

2. Pérez Berrocal, D. A., Witting, K. F., Ovaa, H., and Mulder, M. P. C. (2019) Hybrid Chains: A Collaboration of Ubiquitin and Ubiquitin-Like Modifiers Introducing Cross-Functionality to the Ubiquitin Code. *Front Chem*. **7**, 931
3. Wang, L., Sun, X., He, J., and Liu, Z. (2021) Functions and Molecular Mechanisms of Deltex Family Ubiquitin E3 Ligases in Development and Disease. *Front Cell Dev Biol*. **9**, 706997
4. Yan, Q., Dutt, S., Xu, R., Graves, K., Juszczynski, P., Manis, J. P., and Shipp, M. A. (2009) BBAP monoubiquitylates histone H4 at lysine 91 and selectively modulates the DNA damage response. *Mol Cell*. **36**, 110–120
5. Chatrin, C., Gabrielsen, M., Buetow, L., Nakasone, M. A., Ahmed, S. F., Sumpton, D., Sibbet, G. J., Smith, B. O., and Huang, D. T. (2020) Structural insights into ADP-ribosylation of ubiquitin by Deltex family E3 ubiquitin ligases. *Sci Adv*. 10.1126/sciadv.abc0418
6. Ashok, Y., Vela-Rodríguez, C., Yang, C., Alanen, H. I., Liu, F., Paschal, B. M., and Lehtiö, L. (2022) Reconstitution of the DTX3L-PARP9 complex reveals determinants for high-affinity heterodimerization and multimeric assembly. *Biochem J*. **479**, 289–304
7. Yan, Q., Xu, R., Zhu, L., Cheng, X., Wang, Z., Manis, J., and Shipp, M. A. (2013) BAL1 and its partner E3 ligase, BBAP, link Poly(ADP-ribose) activation, ubiquitylation, and double-strand DNA repair independent of ATM, MDC1, and RNF8. *Mol Cell Biol*. **33**, 845–857
8. Vela-Rodríguez, C., and Lehtiö, L. (2022) Activities and binding partners of E3 ubiquitin ligase DTX3L and its roles in cancer. *Biochem Soc Trans*. **50**, 1683–1692
9. Clague, M. J., Urbé, S., and Komander, D. (2019) Breaking the chains: deubiquitylating enzyme specificity begets function. *Nat Rev Mol Cell Biol*. **20**, 338–352
10. Hermanns, T., and Hofmann, K. (2023) Bioinformatical Approaches to the Discovery and Classification of Novel Deubiquitinases. *Methods Mol Biol*. **2591**, 135–149
11. Sauer, F., Klemm, T., Kollampally, R. B., Tessmer, I., Nair, R. K., Popov, N., and Kisker, C. (2019) Differential Oligomerization of the Deubiquitinases USP25 and USP28 Regulates Their Activities. *Mol Cell*. **74**, 421-435.e10
12. Knobel, P. A., Belotserkovskaya, R., Galanty, Y., Schmidt, C. K., Jackson, S. P., and Stracker, T. H. (2014) USP28 is recruited to sites of DNA damage by the tandem BRCT domains of 53BP1 but plays a minor role in double-strand break metabolism. *Mol Cell Biol*. **34**, 2062–2074
13. Zhang, D., Zaugg, K., Mak, T. W., and Elledge, S. J. (2006) A role for the deubiquitinating enzyme USP28 in control of the DNA-damage response. *Cell*. **126**, 529–542
14. Müller, I., Strozyk, E., Schindler, S., Beissert, S., Oo, H. Z., Sauter, T., Lucarelli, P., Raeth, S., Hausser, A., Al Nakouzi, N., Fazli, L., Gleave, M. E., Liu, H., Simon, H.-U., Walczak, H., Green, D. R., Bartek, J., Daugaard, M., and Kulms, D. (2020) Cancer Cells Employ Nuclear Caspase-8 to Overcome the p53-Dependent G2/M Checkpoint through Cleavage of USP28. *Mol Cell*. **77**, 970-984.e7
15. Du, S.-C., Zhu, L., Wang, Y.-X., Liu, J., Zhang, D., Chen, Y.-L., Peng, Q., Liu, W., and Liu, B. (2019) SENP1-mediated deSUMOylation of USP28 regulated HIF-1α accumulation and activation during hypoxia response. *Cancer Cell Int*. **19**, 4
16. Fong, C. S., Mazo, G., Das, T., Goodman, J., Kim, M., O'Rourke, B. P., Izquierdo, D., and Tsou, M.-F. B. (2016) 53BP1 and USP28 mediate p53-dependent cell cycle arrest in response to centrosome loss and prolonged mitosis. *Elife*. **5**, e16270
17. Cuella-Martin, R., Oliveira, C., Lockstone, H. E., Snellenberg, S., Grolmusova, N., and Chapman, J. R. (2016) 53BP1 Integrates DNA Repair and p53-Dependent Cell Fate Decisions via Distinct Mechanisms. *Mol Cell*. **64**, 51–64

18. Flügel, D., Görlach, A., and Kietzmann, T. (2012) GSK-3β regulates cell growth, migration, and angiogenesis via Fbw7 and USP28-dependent degradation of HIF-1α. *Blood*. **119**, 1292–1301
19. Wang, X., Liu, Z., Zhang, L., Yang, Z., Chen, X., Luo, J., Zhou, Z., Mei, X., Yu, X., Shao, Z., Feng, Y., Fu, S., Zhang, Z., Wei, D., Jia, L., Ma, J., and Guo, X. (2018) Targeting deubiquitinase USP28 for cancer therapy. *Cell Death Dis*. **9**, 186
20. Richter, K., Paakkola, T., Mennerich, D., Kubaichuk, K., Konzack, A., Ali-Kippari, H., Kozlova, N., Koivunen, P., Haapasaari, K.-M., Jukkola-Vuorinen, A., Teppo, H.-R., Dimova, E. Y., Bloigu, R., Szabo, Z., Kerkelä, R., and Kietzmann, T. (2018) USP28 Deficiency Promotes Breast and Liver Carcinogenesis as well as Tumor Angiogenesis in a HIF-independent Manner. *Mol Cancer Res*. **16**, 1000–1012
21. Popov, N., Wanzel, M., Madiredjo, M., Zhang, D., Beijersbergen, R., Bernards, R., Moll, R., Elledge, S. J., and Eilers, M. (2007) The ubiquitin-specific protease USP28 is required for MYC stability. *Nat Cell Biol*. **9**, 765–774
22. Taranets, L., Zhu, J., Xu, W., and Popov, N. (2015) Fbw7 and Usp28 - enemies and allies. *Mol Cell Oncol*. **2**, e995041
23. Wrigley, J. D., Gavory, G., Simpson, I., Preston, M., Plant, H., Bradley, J., Goeppert, A. U., Rozycka, E., Davies, G., Walsh, J., Valentine, A., McClelland, K., Odrzywol, K. E., Renshaw, J., Boros, J., Tart, J., Leach, L., Nowak, T., Ward, R. A., Harrison, T., and Andrews, D. M. (2017) Identification and Characterization of Dual Inhibitors of the USP25/28 Deubiquitinating Enzyme Subfamily. *ACS Chem Biol*. **12**, 3113–3125
24. Guirouilh-Barbat, J., Rass, E., Plo, I., Bertrand, P., and Lopez, B. S. (2007) Defects in XRCC4 and KU80 differentially affect the joining of distal nonhomologous ends. *Proc Natl Acad Sci U S A*. **104**, 20902–20907
25. Ciccia, A., and Elledge, S. J. (2010) The DNA damage response: making it safe to play with knives. *Mol Cell*. **40**, 179–204
26. Sfeir, A., and Symington, L. S. (2015) Microhomology-Mediated End Joining: A Back-up Survival Mechanism or Dedicated Pathway? *Trends Biochem Sci*. **40**, 701–714
27. Akyüz, N., Boehden, G. S., Süsse, S., Rimek, A., Preuss, U., Scheidtmann, K.-H., and Wiesmüller, L. (2002) DNA substrate dependence of p53-mediated regulation of double-strand break repair. *Mol Cell Biol*. **22**, 6306–6317
28. Keimling, M., Deniz, M., Varga, D., Stahl, A., Schrezenmeier, H., Kreienberg, R., Hoffmann, I., König, J., and Wiesmüller, L. (2012) The power of DNA double-strand break (DSB) repair testing to predict breast cancer susceptibility. *FASEB J*. **26**, 2094–2104
29. Bennardo, N., Cheng, A., Huang, N., and Stark, J. M. (2008) Alternative-NHEJ is a mechanistically distinct pathway of mammalian chromosome break repair. *PLoS Genet*. **4**, e1000110
30. Juszczynski, P., Kutok, J. L., Li, C., Mitra, J., Aguiar, R. C. T., and Shipp, M. A. (2006) BAL1 and BBAP are regulated by a gamma interferon-responsive bidirectional promoter and are overexpressed in diffuse large B-cell lymphomas with a prominent inflammatory infiltrate. *Mol. Cell. Biol.* **26**, 5348–5359
31. Holleman, J., and Marchese, A. (2014) The ubiquitin ligase deltex-3l regulates endosomal sorting of the G protein-coupled receptor CXCR4. *Mol Biol Cell*. **25**, 1892–1904
32. Liu, C., Vyas, A., Kassab, M. A., Singh, A. K., and Yu, X. (2017) The role of poly ADP-ribosylation in the first wave of DNA damage response. *Nucleic Acids Res*. **45**, 8129–8141
33. Wei, H., and Yu, X. (2016) Functions of PARylation in DNA Damage Repair Pathways. *Genomics Proteomics Bioinformatics*. **14**, 131–139

34. Aguiar, R. C. T., Takeyama, K., He, C., Kreinbrink, K., and Shipp, M. A. (2005) B-aggressive lymphoma family proteins have unique domains that modulate transcription and exhibit poly(ADP-ribose) polymerase activity. *J. Biol. Chem.* **280**, 33756–33765
35. Lüscher, B., Ahel, I., Altmeyer, M., Ashworth, A., Bai, P., Chang, P., Cohen, M., Corda, D., Dantzer, F., Daugherty, M. D., Dawson, T. M., Dawson, V. L., Deindl, S., Fehr, A. R., Feijs, K. L. H., Filippov, D. V., Gagné, J.-P., Grimaldi, G., Guettler, S., Hoch, N. C., Hottiger, M. O., Korn, P., Kraus, W. L., Ladurner, A., Lehtiö, L., Leung, A. K. L., Lord, C. J., Mangerich, A., Matic, I., Matthews, J., Moldovan, G.-L., Moss, J., Natoli, G., Nielsen, M. L., Niepel, M., Nolte, F., Pascal, J., Paschal, B. M., Pawłowski, K., Poirier, G. G., Smith, S., Timinszky, G., Wang, Z.-Q., Yélamos, J., Yu, X., Zaja, R., and Ziegler, M. (2022) ADP-ribosyltransferases, an update on function and nomenclature. *FEBS J.* **289**, 7399–7410
36. Yang, C.-S., Jividen, K., Spencer, A., Dworak, N., Ni, L., Oostdyk, L. T., Chatterjee, M., Kuśmider, B., Reon, B., Parlak, M., Gorbunova, V., Abbas, T., Jeffery, E., Sherman, N. E., and Paschal, B. M. (2017) Ubiquitin Modification by the E3 Ligase/ADP-Ribosyltransferase Dtx3L/Parp9. *Mol. Cell*. **66**, 503-516.e5
37. Kamata, T., Yang, C.-S., and Paschal, B. M. (2021) PARP7 mono-ADP-ribosylates the agonist conformation of the androgen receptor in the nucleus. *Biochem J*. **478**, 2999–3014
38. Zhen, Y., Knobel, P. A., Stracker, T. H., and Reverter, D. (2014) Regulation of USP28 deubiquitinating activity by SUMO conjugation. *J Biol Chem*. **289**, 34838–34850
39. Mazzucco, A. E., Smogorzewska, A., Kang, C., Luo, J., Schlabach, M. R., Xu, Q., Patel, R., and Elledge, S. J. (2017) Genetic interrogation of replicative senescence uncovers a dual role for USP28 in coordinating the p53 and GATA4 branches of the senescence program. *Genes Dev*. **31**, 1933–1938
40. Kim, H., Kim, D., Choi, H., Shin, G., and Lee, J.-K. (2022) Deubiquitinase USP2 stabilizes the MRE11-RAD50-NBS1 complex at DNA double-strand break sites by counteracting the ubiquitination of NBS1. *J Biol Chem*. **299**, 102752
41. Bartosova, Z., and Krejci, L. (2014) Nucleases in homologous recombination as targets for cancer therapy. *FEBS Lett*. **588**, 2446–2456
42. Dahm-Daphi, J., Hubbe, P., Horvath, F., El-Awady, R. A., Bouffard, K. E., Powell, S. N., and Willers, H. (2005) Nonhomologous end-joining of site-specific but not of radiation-induced DNA double-strand breaks is reduced in the presence of wild-type p53. *Oncogene*. **24**, 1663–1672
43. Wang, Y.-H., Ho, T. L. F., Hariharan, A., Goh, H. C., Wong, Y. L., Verkaik, N. S., Lee, M. Y., Tam, W. L., van Gent, D. C., Venkitaraman, A. R., Sheetz, M. P., and Lane, D. P. (2022) Rapid recruitment of p53 to DNA damage sites directs DNA repair choice and integrity. *Proc Natl Acad Sci U S A*. **119**, e2113233119
44. Schellenbauer, A., Guilly, M.-N., Grall, R., Le Bars, R., Paget, V., Kortulewski, T., Sutcu, H., Mathé, C., Hullo, M., Biard, D., Leteurtre, F., Barroca, V., Corre, Y., Irbah, L., Rass, E., Theze, B., Bertrand, P., Demmers, J. A. A., Guirouilh-Barbat, J., Lopez, B. S., Chevillard, S., and Delic, J. (2021) Phospho-Ku70 induced by DNA damage interacts with RNA Pol II and promotes the formation of phospho-53BP1 foci to ensure optimal cNHEJ. *Nucleic Acids Res*. **49**, 11728–11745
45. Obermeier, K., Sachsenweger, J., Friedl, T. W. P., Pospiech, H., Winqvist, R., and Wiesmüller, L. (2016) Heterozygous PALB2 c.1592delT mutation channels DNA double-strand break repair into error-prone pathways in breast cancer patients. *Oncogene*. **35**, 3796–3806
46. Parameswaran, B., Chiang, H.-C., Lu, Y., Coates, J., Deng, C.-X., Baer, R., Lin, H.-K., Li, R., Paull, T. T., and Hu, Y. (2015) Damage-induced BRCA1 phosphorylation by Chk2 contributes to the timing of end resection. *Cell Cycle*. **14**, 437–448

47. Lim, J. W., Kim, H., and Kim, K. H. (2002) Expression of Ku70 and Ku80 mediated by NF-kappa B and cyclooxygenase-2 is related to proliferation of human gastric cancer cells. *J Biol Chem*. **277**, 46093–46100
48. Volcic, M., Karl, S., Baumann, B., Salles, D., Daniel, P., Fulda, S., and Wiesmüller, L. (2012) NF-κB regulates DNA double-strand break repair in conjunction with BRCA1-CtIP complexes. *Nucleic Acids Res*. **40**, 181–195
49. Wu, K., Jiang, S. W., Thangaraju, M., Wu, G., and Couch, F. J. (2000) Induction of the BRCA2 promoter by nuclear factor-kappa B. *J Biol Chem*. **275**, 35548–35556
50. De Siervi, A., De Luca, P., Moiola, C., Gueron, G., Tongbai, R., Chandramouli, G. V. R., Haggerty, C., Dzekunova, I., Petersen, D., Kawasaki, E., Kil, W. J., Camphausen, K., Longo, D., and Gardner, K. (2009) Identification of new Rel/NFkappaB regulatory networks by focused genome location analysis. *Cell Cycle*. **8**, 2093–2100
51. Multhoff, G., and Vaupel, P. (2020) Hypoxia Compromises Anti-Cancer Immune Responses. *Adv Exp Med Biol*. **1232**, 131–143
52. Solvie, D., Baluapuri, A., Uhl, L., Fleischhauer, D., Endres, T., Papadopoulos, D., Aziba, A., Gaballa, A., Mikicic, I., Isaakova, E., Giansanti, C., Jansen, J., Jungblut, M., Klein, T., Schülein-Völk, C., Maric, H., Doose, S., Sauer, M., Beli, P., Rosenwald, A., Dobbelstein, M., Wolf, E., and Eilers, M. (2022) MYC multimers shield stalled replication forks from RNA polymerase. *Nature*. **612**, 148–155
53. Gaciarz, A., Veijola, J., Uchida, Y., Saaranen, M. J., Wang, C., Hörkkö, S., and Ruddock, L. W. (2016) Systematic screening of soluble expression of antibody fragments in the cytoplasm of E. coli. *Microb Cell Fact*. **15**, 22
54. Lim, K. L., Chew, K. C. M., Tan, J. M. M., Wang, C., Chung, K. K. K., Zhang, Y., Tanaka, Y., Smith, W., Engelender, S., Ross, C. A., Dawson, V. L., and Dawson, T. M. (2005) Parkin mediates nonclassical, proteasomal-independent ubiquitination of synphilin-1: implications for Lewy body formation. *J Neurosci*. **25**, 2002–2009
55. Immenschuh, S., Hinke, V., Ohlmann, A., Gifhorn-Katz, S., Katz, N., Jungermann, K., and Kietzmann, T. (1998) Transcriptional activation of the haem oxygenase-1 gene by cGMP via a cAMP response element/activator protein-1 element in primary cultures of rat hepatocytes. *Biochem J*. **334 (Pt 1)**, 141–146
56. Deniz, M., Kaufmann, J., Stahl, A., Gundelach, T., Janni, W., Hoffmann, I., Keimling, M., Hampp, S., Ihle, M., and Wiesmüller, L. (2016) In vitro model for DNA double-strand break repair analysis in breast cancer reveals cell type-specific associations with age and prognosis. *FASEB J*. **30**, 3786–3799